Global simulations of tokamak microturbulence: finite-β effects and collisions.

A. Bottino[1], T. Vernay[2], B. Scott[1], S. Brunner [2], R. Hatzky[1], S. Jolliet[2], B.F. McMillan[3], T.M. Tran[2], L. Villard[2]

[1] Max-Planck-Institut für Plasmaphysik, EURATOM Association, 85748 Garching, Germany

[2] Centre de Recherches en Physique des Plasmas, Association Euratom - Conf. Suisse, EPFL, Lausanne, Switzerland

[3] Centre for Fusion, Space and Astrophysics, department of physics, University of Warwick, CV4 7AL, Coventry UK

E-mail: bottino@ipp.mpg.de

Abstract. In this paper we present global nonlinear gyrokinetic simulations including finite β_e effects and collisions in tokamak geometry. Global electromagnetic simulations using conventional δf particle in cell methods are very demanding, with respect to numerical resources, in order to correctly describe the evolution of the nonadiabatic part of the electron distribution function. This difficulty has been overcome by using an appropriate adjustable control variate method in the conventional δf scheme. Linearized inter-species and like-species collision operators have also been introduced in the model. The inclusion of the collisional dynamics makes it possible to carry out simulations of microturbulence starting from a global neoclassical equilibrium and to study the effect of collisions on the transport induced by electrostatic microinstabilities.

1. Introduction

The theoretical understanding of mesoscale and microscale turbulence is required for developing a predictive capability of heat, particle and momentum transport in tokamaks and stellarators. Many global linear and nonlinear particle in cell (PIC) codes are routinely used for solving the gyrokinetic equations in the limit of the electrostatic approximation. However, the electrostatic approximation is expected to break down in the core of high β_{e} ($\beta_{\mathrm{e}} \equiv \mu_0 n_{\mathrm{e}} T_{\mathrm{e}}/B^2$) plasmas or in any region where pressure gradients are large. For a finite value of β_{e}, magnetic fluctuations modify the evolution of the electrostatic instabilities and eventually introduce new electromagnetic modes [1]. Therefore, a complete electromagnetic treatment of plasma instabilities is desirable and must be included in models and codes. Most of the existing gyrokinetic PIC codes are based on the δf method [2, 3, 4]. In the δf method the distribution function f of each plasma species is split into a time independent background distribution function f_0 and a time dependent perturbation δf, $f = f_0 + \delta f$. In the δf method, the perturbed part only (δf) is discretized using numerical particles. As long as the perturbation δf remains small as compared to f_0, the δf method reduces the statistical noise. The δf method can be interpreted as a "control variate" algorithm [5, 6], a variance reduction technique widely used for Monte Carlo methods. Electromagnetic simulations using a conventional δf method are much more demanding in respect of numerical resources than electrostatic simulations. The parallel electron dynamics imposes a strong constraint on the size of the time step. In addition to this, electromagnetic simulations require a much larger number of numerical particles in order to correctly describe the evolution of the non-adiabatic part of the electron distribution function. Indeed, the physically relevant non-adiabatic part of the electron distribution function is overwhelmed by the adiabatic response to the magnetic potential $A_{\parallel}$ leading to a severe accuracy problem, known in the literature as the "cancellation problem" (see [6] and references therein). Two main methods have been proposed to overcome those difficulties: the so called "split-weight" scheme, originally proposed in [7], and the use of an appropriate adjustable control variate method in the conventional δf scheme [6]. The adjustable control variate method has been applied in linear electromagnetic tokamak simulations using the code GYGLES [8]. The same method has been successfully extended to nonlinear simulations using NEMORB[9], a new electromagnetic, multispecies version of the code ORB5 [10]. The inclusion of realistic collision operators introduces real physical dissipation, leading to steady state simulations with effects on microinstability dispersion and consequently on the turbulent transport. Since zonal flows are damped by collisions , the inclusion of collision operators can lead to different transport levels with respect to collisionless simulation for ion scale microinstabilities. The organization of the paper is as follows. In Sec.II the gyrokinetic model used in the codes is presented. Section III is dedicated to the numerical discretization of parallel Ampère's law. Nonlinear simulations of finite-β_{e} microturbulence are presented in section IV. Section V gives a brief introduction to the inclusion of collisions in the code, including neoclassical validations and preliminary

results of turbulence simulations.

2. Overview and discretization of the gyrokinetic model

Our gyrokinetic model is based on the gyrokinetic Vlasov-Maxwell system of equations of Hahm and Brizard [11, 12, 13, 14]. The latter consists of a set of self-consistent and energy conserving nonlinear gyrokinetic equations for particles and fields.
The particle Lagrangian is

$$L \equiv (e\mathbf{A} + p_z\mathbf{b}) \cdot \dot{\mathbf{R}} + \frac{m^2}{e}\mu\dot{\theta} - H \tag{1}$$

where $(\mathbf{R}, p_z, \mu, \theta)$ are the particle coordinates, $\mathbf{b}$ is the unit vector for $\mathbf{B}$, m and e are the species mass and charge. Here, $\mu \equiv v_\perp^2/2B$ is magnetic moment per unit mass and p_z is the canonical parallel momentum coordinate, defined by:

$$mU \equiv p_z - eJ_0A_\parallel \quad , \qquad U = \frac{\partial H}{\partial p_z} \tag{2}$$

U is the parallel velocity of the particle and J_0 is the gyroaverage operator.
The Hamiltonian contains only terms up to the first order in the potential fields, Φ and $A_\parallel$:

$$H = m\frac{U^2}{2} + m\mu B + eJ_0\Phi + \mathcal{O}(\Phi^2) \simeq \frac{p_z^2}{2m} + m\mu B + e\left(J_0\Phi - \frac{p_z}{m}J_0A_\parallel\right) \quad .(3)$$

The equations of motion are given by the Euler-Lagrange equations:

$$\dot{\mathbf{R}} = \frac{\partial H}{\partial p_z}\frac{\mathbf{B}^*}{B_\parallel^*} - \frac{1}{eBB_\parallel^*}\mathbf{F}\cdot\nabla H \tag{4}$$

$$\dot{p_z} = -\frac{\mathbf{B}^*}{B_\parallel^*}\cdot\nabla H \tag{5}$$

we have used a tensor notation for the magnetic field, summarized by:

$$\mathbf{F} = \nabla\mathbf{A} - (\nabla\mathbf{A})^T \quad \mathbf{F} = \epsilon\cdot\mathbf{B} \quad \nabla\times\mathbf{b} = -\nabla\cdot\frac{\mathbf{F}}{B} \quad \mathbf{b}\times = -\frac{\mathbf{F}}{B}\cdot \quad . \tag{6}$$

Replacing the Hamiltonian of Eq. (3) in the Euler-Lagrange equations (4) and defining a generalized potential Ψ, the equations of motion become:

$$\begin{aligned}
\Psi &\equiv \Phi - \frac{p_z}{m}A_\parallel \\
\dot{\mathbf{R}} &= \left(\frac{p_z}{m} - \frac{e}{m}J_0A_\parallel\right)\frac{\mathbf{B}^*}{B_\parallel^*} + \frac{1}{B_\parallel^*}\mathbf{b}\times\left[\mu\frac{m}{e}\nabla B + \nabla J_0\Psi\right] \\
\dot{p_z} &= -\frac{m\mathbf{B}^*}{B_\parallel^*}\cdot\left[\mu\nabla B + \frac{e}{m}\nabla J_0\Psi\right]
\end{aligned} \tag{7}$$

where $\mathbf{B}^* = \nabla\times\mathbf{A}^*$ and $\mathbf{A}^* \equiv \mathbf{A} + (p_z/e)\mathbf{b}$. .
The gyrokinetic Vlasov equation is:

$$\frac{\mathrm{D}f}{\mathrm{D}t} = \frac{\partial f}{\partial\mathbf{R}}\cdot\dot{\mathbf{R}} + \frac{\partial f}{\partial p_z}\dot{p_z} = C(f) + S \tag{8}$$

where $f(\mathbf{R}, p_z, \mu)$ is the distribution function of the gyrocenters, $C(f)$ is a collision operator and S is a source term. The time evolution of the perturbed electrostatic potential is described by the quasineutraliy condition (also called polarization equation, or gyrokinetic Poisson equation) in the long wavelength approximation $(k_\perp \rho)^2 \ll 1$ [10]:

$$-\nabla_\perp \left(\sum_{\text{species}} \frac{m n_0}{e B^2} \right) \nabla_\perp \Phi = \sum_{\text{species}} \delta n \tag{9}$$

where $\delta n = \int \mathrm{d}W \; \delta f \delta(\mathbf{R}+\boldsymbol{\rho}-\mathbf{x})$ is the perturbed gyrocenter density, $\boldsymbol{\rho}$ is the gyroradius and $\mathrm{d}W \equiv B_\parallel^* \mathrm{d}\mathbf{R}\mathrm{d}p_z\mathrm{d}\mu\mathrm{d}\theta$. The linearized gyrokinetic parallel Ampère's law determines the evolution of the magnetic potential:

$$\nabla_\perp^2 A_\parallel = \mu_0 \sum_{\text{species}} j_\parallel \tag{10}$$

where $j_\parallel$ is the current density linearized on the background Maxwellian f_0:

$$j_\parallel = e \int \mathrm{d}W \delta(\mathbf{R}+\boldsymbol{\rho}-\mathbf{x}) p_z \left[f - \frac{e p_z}{T} f_0 J_0 A_\parallel \right] \quad . \tag{11}$$

Equation (10) can be rewritten as:

$$\left(\sum_{\text{species}} \frac{\mu_0 n_0 e^2}{m} \langle A_\parallel \rangle \right) - \nabla_\perp^2 A_\parallel = \mu_0 \sum_{\text{species}} \delta j_\parallel \tag{12}$$

where $\delta j_\parallel = e \int \mathrm{d}W (p_z/m) \delta f \delta(\mathbf{R}+\boldsymbol{\rho}-\mathbf{x})$ and $\langle A_\parallel \rangle \equiv (n_0)^{-1} \int \mathrm{d}W f_0 J_0 A_\parallel \delta(\mathbf{R}+\boldsymbol{\rho}-\mathbf{x})$. For $C(F) = 0$ and $S = 0$, the set of gyrokinetic equations given by (7,8,9,12) is energy and momentum conserving. An elegant proof is given in Ref. [15].
Defining for a species s the thermal gyroradius, $\rho_s \equiv \sqrt{m_s T_s}/(eB_0)$, and the plasma β, $\beta_s = \mu_0 n_0 T / B_0^2$, equation (12) becomes, for a single ion species:

$$\frac{\beta_s}{\rho_s^2} \langle A_\parallel \rangle_s + \frac{\beta_e}{\rho_e^2} \langle A_\parallel \rangle_e - \nabla_\perp^2 A_\parallel = \mu_0 \sum_{\text{species}} \delta j_\parallel \quad . \tag{13}$$

The p_z formulation implies the appearance of large unphysical terms in the parallel Ampère's law (13). Considering the Hamiltonian (3), one can define the adiabatic part of the distribution function as

$$F^{\text{ad}} \equiv -\frac{e f_0}{T} (J_0 \Phi - p_z J_0 A_\parallel) \quad , \tag{14}$$

and an adiabatic current $j_\parallel^{\text{ad}}$:

$$\begin{aligned} \mu_0 j_\parallel^{\text{ad}} &\equiv \mu_0 e \int \mathrm{d}W \delta(\mathbf{R}+\boldsymbol{\rho}-\mathbf{x}) F^{\text{ad}} p_z \\ &= \mu_0 e \int \mathrm{d}W \delta(\mathbf{R}+\boldsymbol{\rho}-\mathbf{x}) \frac{e f_0 p_z^2}{T} J_0 A_\parallel = \frac{\beta_s}{\rho_s^2} \langle A_\parallel \rangle \end{aligned} \tag{15}$$

Therefore, the adiabatic component of the current corresponds exactly to the skin term on the left hand side of (13). In a particle in cell simulation, the currents are discretized with markers, while the skin terms are constructed analytically on a fixed grid. The unavoidable inaccuracy due to the different discretizations leads to an inexact cancellation of the two terms and potentially large errors in the simulation (cancellation

problem). More details can be found in [8, 6]. Due to the structure of the equation, the cancellation problem becomes more severe with increasing β_s and decreasing $k_\perp$. In the long wavelength approximation, the parallel Ampère's law becomes [8]:

$$\left(\sum_{\text{species}} \frac{\mu_0 n_0 e^2}{m} A_\parallel\right) - \nabla_\perp^2 A_\parallel + \left(\sum_{\text{species}} \nabla_\perp \frac{\mu_0 n_0 T}{B_0^2} \nabla_\perp A_\parallel\right) = \mu_0 \sum_{\text{species}} \delta j_\parallel \quad .(16)$$

In our model, electrons can be treated as kinetic, following a Vlasov equation similar to Eq. (8) with $J_0 \equiv 1$, or as adiabatic, assuming $n_e \simeq e\phi/T_e$. Alternatively, a hybrid model for electrons can be used, were only trapped electrons are drift kinetic, while passing electrons respond adiabatically to the perturbation [16]. Figure 1 shows a comparisons between the fully kinetic model for electrons and the hybrid model. Here, the growth rate of a trapped electron mode (TEM) is plotted as a function of the ion to electron mass ratio. The hybrid model recovers the correct value of γ for smaller mass ratio and, therefore, larger time step. In addition, to this, the hybrid model avoids severe numerical instabilities, associated with the parallel motion of the passing electrons, which further limit the simulation time step. A typical example is the so-called omega-H mode, the electrostatic limit of the shear Alfvén wave, driven unstable by the numerical discretization when passing electrons are treated kinetically [17, 18]. The same model has been applied to the linear study of trapped electron modes in ASDEX-Upgrade [19] and TCV discharges [20].

3. Numerical discretization

The complete discretization of the electrostatic model is described in [10], here we report the details of the discretization of the parallel Ampère's law only. Following the formalism of [6], the parallel potential is discretized using B-splines:

$$A_\parallel(\mathbf{x}, t) = \sum_\mu \phi_\mu(t) \Lambda_\mu(\mathbf{x}) \tag{17}$$

where $\Lambda_\mu(\mathbf{x})$ is a tensor products of 1D B-splines. Using the Galerkin's method, equation (16) can be written in matrix form as:

$$(\hat{\mathbf{L}} + \hat{\mathbf{S}}_\mathbf{i} + \hat{\mathbf{S}}_\mathbf{e})\boldsymbol{\phi} = \mu_0(\mathbf{j}_{\parallel\mathbf{i}} + \mathbf{j}_{\parallel\mathbf{e}}) \tag{18}$$

In the following, the "hat" quantities are matrices, $\boldsymbol{\phi}$ is the B-spline coefficient vector to be solved for and the $\mathbf{j}_\parallel$'s are the coefficient vectors after current-assignment of the weights. The matrix elements of Eq. (18) are defined by

$$\hat{L}_{kj} \equiv \int (1 - \beta_\mathrm{i}) \nabla_\perp \Lambda_j \cdot \nabla_\perp \Lambda_k \mathrm{d}\mathbf{x} \tag{19}$$

$$\hat{S}_{i,kj} \equiv \int \frac{\beta_\mathrm{i}}{\rho_\mathrm{i}^2} \Lambda_j \Lambda_k \mathrm{d}\mathbf{x} \tag{20}$$

$$\hat{S}_{e,kj} \equiv \int \frac{\beta_e}{\rho_e^2} \Lambda_j \Lambda_k \mathrm{d}\mathbf{x} \tag{21}$$

and the current-assignment vectors are:

$$j_{\|\mathrm{e},k} = \sum_{p=1}^{N_\mathrm{e}} p_{z,\mathrm{p}} w_{\mathrm{e,p}} \Lambda_k \tag{22}$$

$$j_{\|\mathrm{i},k} = \sum_{p=1}^{N_\mathrm{i}} p_{z,\mathrm{p}} w_{\mathrm{i,p}} J_0 \Lambda_k \quad ; \tag{23}$$

$w_{e,p}$ and $w_{i,p}$ are the marker weights, for which $\delta f_s = \sum_{p=1}^{N_s} w_s \delta(W - W_\mathrm{p})$ where $W_\mathrm{p} \equiv (\mathbf{R}_\mathrm{p}, p_{z,\mathrm{p}}, \mu_\mathrm{p})$ represents a point in the 5D phase space. N_s is the total number of markers. In order to solve the cancellation problem, we define a "noise reduced" marker weight:

$$\tilde{w}_\mathrm{p} = w_\mathrm{p} - \Omega_\mathrm{p} \frac{e f_0}{T} J_0 A_\| \tag{24}$$

Ω_p is the phase space volume, initially centered around W_p, associated with the marker p (see Ref.[10]). The current-assignment vector, for the new weight $\tilde{w}_\mathrm{p}$ becomes:

$$\mu_0 \tilde{\tilde{\mathbf{j}}}_\| = \mu_0 \mathbf{j}_\| - \mu_0 \hat{\mathbf{j}}_\|^\mathrm{ad} \boldsymbol{\phi} \tag{25}$$

$$\hat{\mathbf{j}}_\|^\mathrm{ad} \boldsymbol{\phi} \equiv \sum_{p=1}^{N_\mathrm{s}} p_{z,p} \Omega_p \frac{e p_z f_0}{T} J_0 A_\| \Lambda_k \tag{26}$$

$$\simeq \mu_0 e \int \mathrm{d}W \delta(\mathbf{R} + \boldsymbol{\rho} - \mathbf{x}) \frac{e f_0 p_z^2}{T} J_0 A_\| \Lambda_k = \hat{\mathbf{S}} \boldsymbol{\phi} \tag{27}$$

having used the definition of adiabatic current of Eq. (15). Since the cancellation problem affects mainly the electrons, noise-reduced weights are used for the electrons only. Therefore, the discretized parallel Ampère's law is:

$$(\hat{\mathbf{L}} + \hat{\mathbf{S}}_\mathrm{i} + \hat{\mathbf{S}}_\mathrm{e}) \boldsymbol{\phi} = \mu_0 \mathbf{j}_{\|\mathrm{i}} + \mu_0 \mathbf{j}_{\|\mathrm{e}} - \hat{\mathbf{j}}_{\|\mathrm{e}}^\mathrm{ad} \boldsymbol{\phi} + \hat{\mathbf{S}}_\mathrm{e} \boldsymbol{\phi} \tag{28}$$

A formal proof of the equivalence of this algorithm with a control variate method is given in [6] (scheme two). This equation can be solved by an iterative procedure (see Appendix B of Ref. [6]).

4. Nonlinear finite β_e simulations of microturbulence in tokamaks

The nonlinear simulations described in this Section, are based on parameters and profiles of the Cyclone base case: $\rho^* = 1/186$ and initial $R/L_T = 9$ between $0.2 < \rho_\mathrm{pol} < 0.8$ for both ions and electrons. A detailed description of the physical parameters and profiles can be found in [21]. The mass ratio is set to $m_\mathrm{i}/m_\mathrm{e} = 1000$ and the value of the central density has been adjusted to have $\beta_\mathrm{e} = 0.3\%$ at the center of the plasma. Figure 2 compares the time evolution of ion thermal diffusivity of a $\beta_\mathrm{e} = 0.3\%$ electromagnetic simulation, with the original electrostatic, adiabatic electrons simulation of Ref. [21] and with an electrostatic simulation using the hybrid model for trapped electrons. The ion thermal diffusivity for the electrostatic simulation including trapped electrons is comparable with the electromagnetic case. The $\beta_\mathrm{e} = 0.3\%$ simulation was performed

using 512 million numerical particles per species and with a time step 20 times smaller than the electrostatic case ($\Delta t = 1\ \Omega_{\rm i}$ where $\Omega_{\rm i}$ is the ion cyclotron frequency). We can observe that the largest effect of the non-adiabatic electron response is due to trapped electrons. A detailed discussion about those simulations can be found in Ref. [9]. In particular, the so called noise-to-signal ratio [22], based on the comparison between the energy in the filtered nonresonant modes, strongly Landau damped, and the energy in the resonant modes, remains below 10% during the entire simulation. The poloidal cross section of the parallel magnetic potential at the end of the simulation is plotted in Fig. 3. The ballooning structure of $A_\parallel$ is still evident and the turbulence eddies appear to be sheared and broken. This is partly due to effect of the mode rational surfaces, and partly to the presence of a strong zonal component of the electrostatic potential. The effect of the zonal flow is particularly evident on the radial structure of the ion heat flux, shown in Fig. 4. Although the initial temperature and density gradients are constant along the minor radius, the heat flux is not constant: the decrease of the flux from the center to the edge is mainly due to the local magnetic shear and the regulating effect of the zonal flow. Figure 4 shows indeed a clear correspondence between the gradient of the zonal flow and the ion heat flux. This is an indication of the basically electrostatic nature (ITG) of the turbulence in this simulation. Figure 5 presents a scan in $\beta_{\rm e}$ for the ion diffusivity; $\beta_{\rm e}$ has been varied by rescaling the value of the density on the axis. A heating source is applied, in order to prevent profile relaxation. The ion diffusivities have been averaged in radius, over the range $\rho_{\rm pol} = [0.6, 0.8]$ ($\rho_{\rm pol}$ is the square root of normalized poloidal flux) and in time, using a moving time window during the stationary phase of the simulations. The stabilizing effect of finite $\beta_{\rm e}$ on ITGs, already documented in many linear simulation, is recovered in global nonlinear simulations.

5. Nonlinear simulations of microturbulence with collisions

The implementation of collision operators in the ORB5 code is described in details in Ref. [23]. The collision operator appearing on the right hand side of the Vlasov equation (8) is linearized with respect to a local Maxwellian $f_{\rm LM} : C(f) \simeq \hat{C}(\delta f_{\rm LM})$ with $\delta f_{\rm LM} = f - f_{\rm LM}$. Moreover, finite Larmor radius effects have been neglected with respect to the collision operators. Electron-ion collisions are described by pitch-angle scattering, modeled by a Lorentz operator, assuming $m_e \ll m_i$. The self-collision operator for both ions and electrons includes the background reaction (of $f_{\rm LM}$ on $\delta f_{\rm LM}$) in a way to preserve conservation of mass, momentum and kinetic energy. Collisions of $\delta f_{\rm LM}$ on $f_{\rm LM}$ are modelled through random kicks of markers in velocity space, following the so-called Langevin approach. The resulting code has been validated against other existing codes on neoclassical transport benchmarks [23]. The statistical noise associated with the particle discretization is amplified in collisional simulations by the weight spreading associated with the diffusive effect of collision operators [24]. Therefore, a noise control scheme based on a coarse graining algorithm [25] has been implemented in the code.

This method is based on a periodic binning of the markers in the 5D gyrokinetic phase space. The weight of each marker in a bin is then modified towards the average weight value of the bin, thus smoothing the distribution function and controlling the numerical noise. It is important to notice that the coarse graining method, not only reduces the statistical noise by reducing the variance of the distribution of the weights, but also introduces dissipation at small scales by limiting the filamentation of the distribution in phase-space. Therefore, it can also be used in collisionless simulations to provide the dissipation necessary to assure entropy saturation and steady state turbulence. The details of the algorithm will be discussed elsewhere. Here we show that the coarse graining method does not modify the spectrum of the turbulence when the size of the bins in $(\rho_{\rm pol},s,\varphi,p_z,\mu)$, s being a coordinate along the field lines, are carefully chosen, as illustrated in Fig. 6.

As a preliminary example of turbulence simulation with collisions, we have studied the Cyclone base case for two different initial temperature gradients $R/L_T = 6.9$ (nominal value) and $R/L_T = 5.3$. Note that $R/L_T = 5.3$ is below the nonlinear critical gradient of the collisionless case. The collisionality $\nu* = 0.45$, used in those simulations, is approximately ten times larger than the physical collisionality of the Cyclone case. The radial profile of the ion heat diffusivity is described in figure 7. For the initial $R/L_T = 6.9$ case, the turbulence induced ion heat diffusivity is larger than the neoclassical one and it is also larger than the ion heat diffusivity of the collisionless case, i.e. $\chi_i/\chi_{GB} \simeq 2$, due to the collisional damping of the zonal flow. In the second case, initial $R/L_T = 5.3$, a turbulence induced heat diffusivity is present only for finite collisionality. This is again consistent with the fact that collisions damp the zonal flow and thus soften the so-called Dimits shift [26]. In this case, the turbulence induced ion heat diffusivity is of the same order of the neoclassical one. Note that the measured neoclassical ion heat diffusivity is comparable with the Chang-Hinton analytical estimate.

6. Conclusions

The parallel component of Ampère's law has been successfully added in the Particle-In-Cell code ORB5 and we have proven that an adjustable control variate method [6] can be used to solve the cancellation problem also in nonlinear simulations. As a result, using all the control techniques available, achievement of converged global nonlinear electromagnetic simulations for the Cyclone base case, now require the same amount of numerical resources than standard electrostatic simulations.

Collisional effects have been also added to the global gyrokinetic code ORB5. The code has been validated against other codes and analytical predictions on neoclassical benchmarks, showing very good agreement. The crucial issue of numerical noise for PIC codes has been addressed through the use of a coarse graining procedure.

References

[1] F Zonca, L Chen, and J Q Dong. *Physics of Plasmas*, 6:1917, 1999.
[2] W W Lee. Gyrokinetic approach in particle simulations. *Physics of Fluids*, 26:556, 1983.
[3] S E Parker and Lee W W. *Physics of Fluids B*, 5:77, 1993.
[4] A M Dimits and W W Lee. *Journal of Computational Physics*, 107:309, 1993.
[5] A Y Aydemir. *Physics of Plasmas*, 1:5480, 1994.
[6] R Hatzky, A Könies, and A Mishchenko. *Journal of Computational Physics*, 189:463, 2007.
[7] Y Chen and S E Parker. *Journal of Computational Physics*, 189:463, 2003.
[8] A Mishchenko, R Hatzky, and A Könies. *Physics of Plasmas*, 11:5480, 2004.
[9] A Bottino, B Scott, S Brunner, et al. *IEEE Transactions on Plasma Science*, 38:2129, 2010.
[10] S Jolliet, A Bottino, P Angelino, et al. *Computer Physics Communications*, 177:409, 2007.
[11] T S Hahm, W W Lee, and A Brizard. *Physics of Fluids*, 31:1940, 1988.
[12] T S Hahm. *Physics of Fluids*, 31:2670, 1988.
[13] A Brizard. *Journal of Plasma Physics*, 41:541, 1989.
[14] H Sugama. *Physics of Plasmas*, 7:466, 2000.
[15] B Scott and J Smirnov. *Physics of Plasmas*, 17:112302, 2010.
[16] S Jolliet. *Gyrokinetic PIC simulations of ITG and CTEM turbulence in tokamaks.* PhD Thesis No.**4326**, Ecole Polytechnique Fédérale de Lausanne, 2005.
[17] W W Lee. *Journal of Computational Physics*, **73**:243, 1987.
[18] S Sorge and R Hatzky. *Physics of Plasmas*, 44:2471, 2002.
[19] A Bottino, A G Peeters, O Sauter, L. Villard, and ASDEX Upgrade Team. **11**:198, 2004.
[20] A Bottino, O Sauter, Y Camenen, and E Fable. *Plasma Physics and Controlled Fusion*, 48(2):215–233, 2006.
[21] G L Falchetto et al. *Plasma Physics and Controlled Fusion*, 50:124015, 2008.
[22] A Bottino, AG Peeters, R Hatzky, S Jolliet, BF McMillan, TM Tran, and L Villard. *Physics of Plasmas*, 14(1), 2007.
[23] T Vernay, S Brunner, L Villard, BF McMillan, S Jolliet, TM Tran, A Bottino, and JP Graves. *Physics of Plasmas*, 17(12), 2010.
[24] S Brunner, E Valeo, and J A Krommes. *Physics of Plasmas*, 6:4504, 1999.
[25] Y Chen and S E Parker. *Physics of Plasmas*, 14:082301, 2007.
[26] H Lin, TS Hahm, WW Lee, Tang WM, and PH Diamond. *Physical Review Letters*, 83:3645, 1999.
[27] A Bottino. *Modelling of global electrostatis microinstabilities in tokamaks: effects of ExB flow and magnetic shear.* PhD Thesis No.**2983**, Ecole Polytechnique Fédérale de Lausanne, 2005.

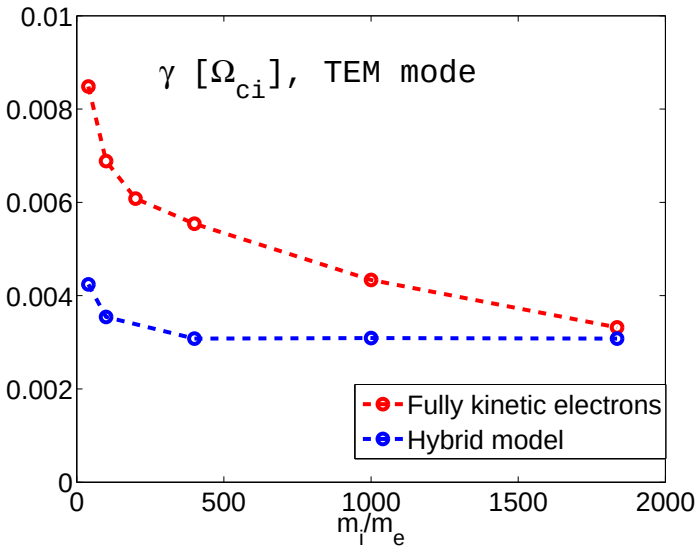

Figure 1. Growth rate of the most unstable mode (TEM), as a function of the ion-electron mass ratio; $\rho_s = 1/60$, $a/L_{\mathrm{T,e}} = 2.50$, $a/L_{\mathrm{T,i}} = 0$. The complete set of physical and numerical parameters can be found in [27], pag.78.

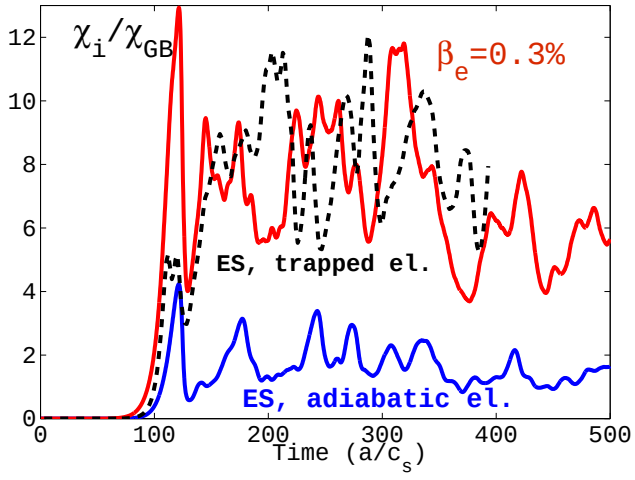

Figure 2. Cyclone base case: time evolution of the ion thermal diffusivity for an electromagnetic $\beta_e = 0.3\%$ simulation (red), the standard electrostatic Cyclone case (red) and the hybrid model for trapped electrons (dashed-black).

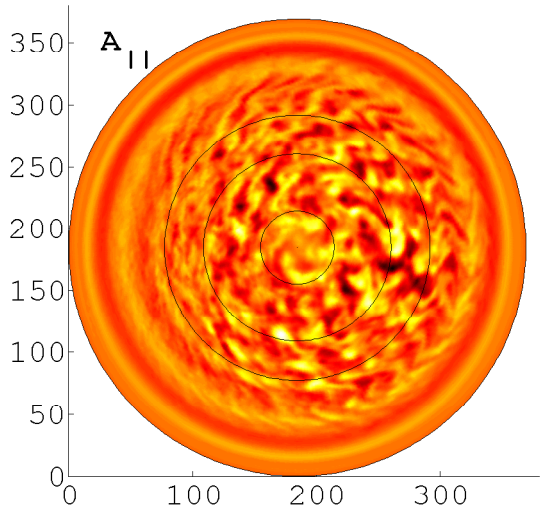

Figure 3. Cyclone base case: poloidal cross section of the magnetic potential at $t = 500[a/c_s]$. The R and Z coordinates are given in $[\rho^{*-1}]$ units. Dashed lined correspond to the $q = [1, 1.2, 2]$ mode rational surfaces. .

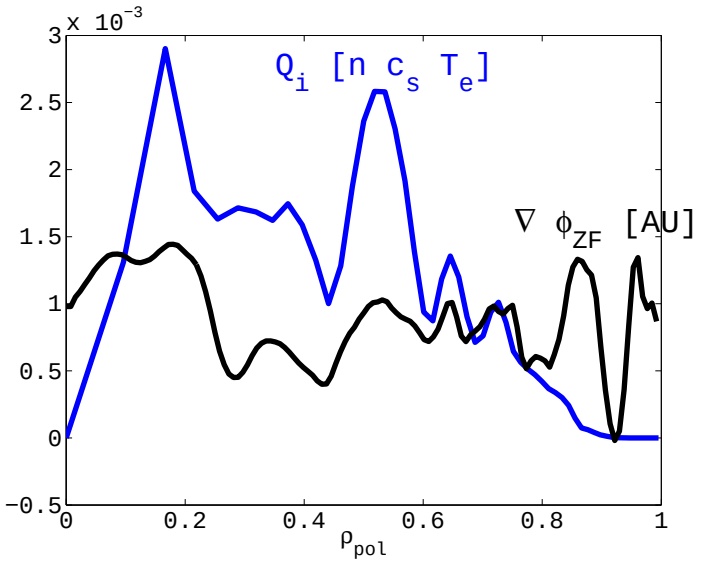

Figure 4. Cyclone base case: radial profile of ion heat flux and of the zonal flow at $t = 500[a/c_s]$.

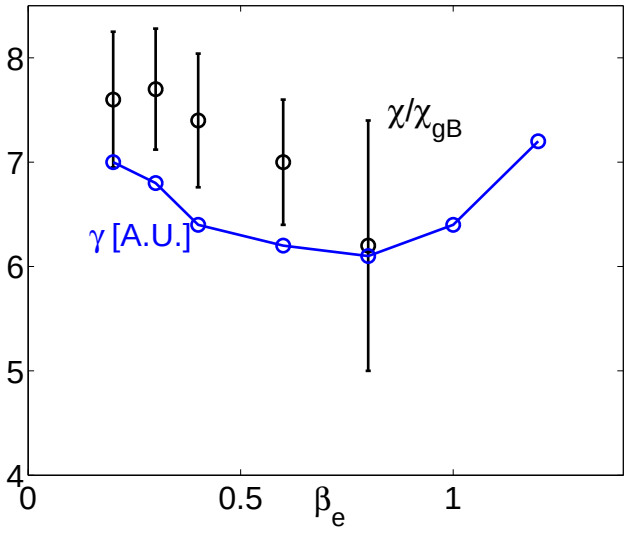

Figure 5. Cyclone base case: ion thermal diffusivity and linear growth rate γ as a function of β_e; error bars: moving averaged in time.

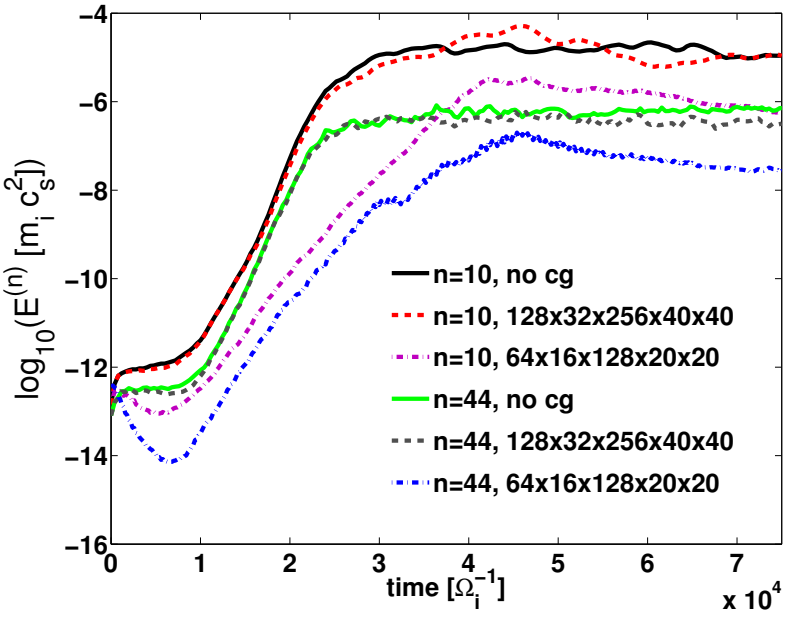

Figure 6. Cyclone base case: time evolution of two different toroidal mode number, n, of the field energy for different choices of the coarse graining grid ($\mathrm{n}\rho_{\mathrm{pol}} \times \mathrm{n}s \times \mathrm{n}\varphi \times \mathrm{n}p_z \times \mathrm{n}\mu$).

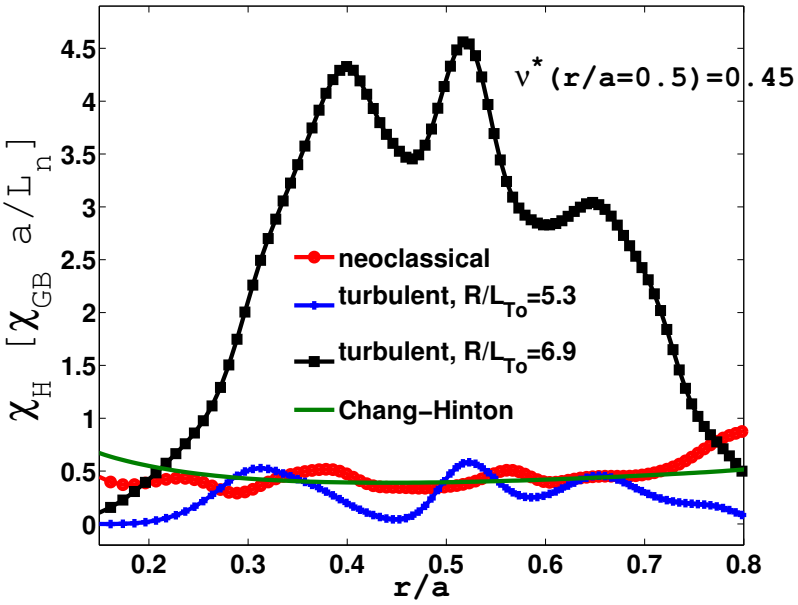

Figure 7. Cyclone base case: radial profile of the ion thermal diffusivity (turbulent and neoclassical) for different value of the initial R/L_T. Green: Chang-Hinton estimate of the neoclassical ion diffusivity.